https://doi.org/10.1016/j.eti.2020.100812

A “classic” material for capture and detoxification of emergent contaminants for water purification: the case of Tetracycline.

Vito Rizzi[a], Jennifer Gubitosa[b], Paola Fini[b], Andrea Petrella[c], Roberto Romita[a], Angela Agostiano[a,b] and Pinalysa Cosma[a,b*]

[a]*Università degli Studi “Aldo Moro” di Bari, Dip. Chimica, Via Orabona, 4- 70126 Bari, Italy.*

[b]*Consiglio Nazionale delle Ricerche CNR-IPCF, UOS Bari, Via Orabona, 4- 70126 Bari, Italy.*

[c]*Dipartimento di Ingegneria Civile, Ambientale, Edile, del Territorio e di Chimica, Politecnico di Bari, Orabona, 4, 70125, Bari, Italy.*

*Corresponding Authors:
Prof. Pinalysa COSMA
Università degli Studi “Aldo Moro” di Bari
Dipartimento di Chimica
Via Orabona, 4
I-70126 Bari, ITALY
e-mail: pinalysa.cosma@uniba.it
tel. +39 0805443443
fax +39 0805442128

Declarations of interest: none.

ABSTRACT

Emerging pollutants are well-known chemicals without regulatory status that produce a significant environmental impact reaching aquatic and land ecosystems with a negative effect in the provision of ecosystem services. The aim of this work is the removal of tetracycline, through adsorption processes, from water by using alginate/chitosan microbeads enriched with TiO_2. Through the photodegradation of the tetracycline, the recycle of the adsorbent is proposed under proper experimental conditions of work. While, by changing the ionic strength, a cleaner and low-cost approach is also presented to recover by desorption the adsorbed pollutant. The adsorption efficiencies observed for chitosan/alginate/TiO_2 composite materials indicate them as suitable for environmental applications, in the perspective of sustainable development and innovations in this field. Further, a detailed physical and chemical investigation is discussed assessing the kinetics and the isotherms of adsorption, along with the thermodynamic parameters.

KEYWORDS: alginate; chitosan; alginate/chitosan beads; TiO_2; emerging pollutants; tetracycline; photodegradation.

1. INTRODUCTION

The idea of “Cleaner Production” took hold in the 1950s and 1960s with the aim of making industry aware of its environmental impact. More specifically, cleaner production indicates the substitution of harmful products by less dangerous ones, together with the development of more efficient industrial processes. However, the Cleaner Production concept was really developed in 1990s, during the Rio conference promoted by United Nations Environmental Program (1992), when the Cleaner Production was defined as “continuous application of an integrated preventive environmental strategy to processes, products, and services to increase efficiency and reduce risks to humans and the environment” (Hens et al., 2018). For environmental applications, a sustainable design aims to reduce the overall impact through the recycle (Kurk and Eagan, 2008). These concepts converge in a wider idea of “Cleaner technologies” which includes various aspects: extraction and use of natural resources, generation of products with reduced or no potentially harmful components, minimization of air, water and soil pollution during fabrication and use of products that should be durable and recyclable (Belayutham et al., 2016). On this ground, the present work reports an example of a cleaner approach, by using natural polymers, to remove/recover emerging pollutants (EPs) from water. Indeed, the contamination of fresh water is a global concern due to the enormous effect of natural and anthropogenic organic substances that are released everyday into the environment (Rizzi et al., 2019a, 2019b). EPs include human and veterinary drugs, disinfectants, fragrances and other compounds commonly employed in medicine, industry, agriculture. For example, drugs can reach the urban wastewater treatment plants after their metabolism and excretion or by their improper dump in toilet sinks as solid wastes (Rizzi et al., 2019a; Safari et al., 2015).

Among drugs, tetracycline (TC), a broad-spectrum antibiotic usually applied to treat diseases in human and veterinary medicine (Chen et al., 2016), is frequently retrieved in wastewater (Yeşilova et al., 2018). Not surprisingly, TCs constitute about the 29% of the used antibiotics (Safari et al., 2015), because they are considered wide range bactericidal agents that inhibit the bacterial protein synthesis (Martins et al., 2015). As reported by Chen et al. (2016), TCs are drugs poorly absorbed in

the digestive tract and they are excreted through feces and urine in original and metabolized forms (Zhu et al., 2014). Consequently, TCs are detected in the soil, sediments, surface water, and drinking water. Moreover, the TC degradation is hard, leading adverse effects on ecosystems and human health, as for example the development of allergies and antibiotic resistance (Chen et al., 2016). Therefore, with the increasing concern for water quality and public health, the development of efficient platforms to monitor and remove TC from water should be highly desirable by applying new sustainable and low-cost wastewater treatment technologies (Zhou et al., 2018; Zhu et al., 2014).

For this purpose, the adsorption methods are still considered the most powerful tools for wastewater treatment (Martins et al., 2015). They are efficient and low-cost approaches that require easy operation for holding pollutants (Martins et al., 2015; Rizzi et al., 2019a, 2019b). Generally activated carbon, biochar, mesoporous silica, zeolite, chitosan, carbon nanotubes, clays, resin, biomass wastes and graphene oxide are reported as common adsorbents to clean water from pharmaceutical pollutants (Martins et al., 2015). Moreover, due to their chemical and physical features, the applications of bio adsorbents for environmental purposes is grown (Abdolmaleki et al., 2018; Lu et al., 2018; Thakur et al., 2018) and the use of alginate and chitosan-based adsorbents appear very interesting (Abdolmaleki et al., 2018; Lu et al., 2018; Semeraro et al., 2017).

Therefore, in this paper, the use of a different adsorbent to remove TC from water is proposed, by using chitosan and alginate polymers. More specifically, a composite adsorbent, with photocatalytic properties, constituted by chitosan coated alginate microbeads (mAL/CH) enriched with commercial TiO_2 P25 Degussa, is efficiently applied. Thanks to their negative charges, alginate polymers tend to gel rapidly and readily crosslink with Calcium ions, forming the well-known “egg-box” three-dimensional structure. On the other hand, Chitosan polymers bind to the alginate’s carboxylate groups ($-COO^-$) through the positively charged protonated amine groups, ($-NH_3^+$), improving the stability and rigidity of the three-dimensional gel structure (Tan et al., 2018). It should be noted that mAL/CH were already successfully used to remove other pollutants from water (Semeraro et al., 2017); so, with the removal of EPs, in particular of TC, the wide range applications of the proposed adsorbent

can be emphasized. In the perspective of a virtuous life cycle, the TC recovery from the adsorbent is also presented under mild experimental conditions by using concentrated salts solutions. For obtaining the recycle of the adsorbent material, the enrichment of the mAL/CH beads with TiO_2 is proposed exploiting its photocatalytic properties using Advanced Oxidation Processes (AOPs) (Jiang et al., 2018; Abdulghani et al., 2013). About this aspect, it should be considered the photostability of the hybrid alginate/chitosan supramolecular assembly under UV irradiation. Indeed, if alginate results to be poorly photostable (in fact, it absorbs energy from UV irradiation forming free radicals able to break the glycosidic bonds inducing the degradation of the polymeric chains (Lam et al., 2017)); on the other hand, as well documented in literature (Liu et al., 2018; Nawi et al., 2011), the chitosan polymer shows a better stability under UV irradiation (Liu et al., 2018; Nawi et al., 2011).

2. MATERIALS AND METHODS

2.1 Chemicals.

All the used chemicals were of analytical grade and samples were prepared using deionized water. Alginic acid sodium salt from brown algae (medium viscosity), calcium chloride ($CaCl_2$), commercial grade chitosan powder (from crab shells, highly viscous, with deacetylation degree ≥75%), Acetic acid (99,9%) and glycerol (+99.5%) were purchased from Sigma-Aldrich. The same commercial source was adopted for Tetracycline (TC: $C_{22}H_{25}N_2O_8$ Cl, M.W. 480,9 g/mol) used without further purification. TC stock solution with a concentration of 1.0×10^{-3} M was prepared. The pH of the various aqueous solutions, when necessary, was adjusted using concentrated HCl and NaOH solutions. Dilutions were performed using deionized water. Aeroxide TiO_2 P25 was purchased from Evonik industries AG.

2.2 Preparation of alginate and alginate-chitosan beads.

Alginate beads (mAL) were prepared using the method of external gelation. AL solution (1% w/v) was extruded dropwise through a needle, with a diameter of 0.8 mm, into calcium chloride solution (2.5% w/v) and the system was maintained under continuous magnetic stirring at room temperature. The needle was placed at the output tube of a peristaltic pump and a constant flow rate (2 mL/min) was used. mAL beads were left in calcium solution for 30 minutes. The beads were collected, repeatedly washed with double distilled water and dried in an oven at 60°C for about 5 hours. To prepare mAL/CH alginate beads, the wet alginate beads were further immersed into chitosan solution (1% w/v) for 60 minutes and maintained under continuous stirring. 100 mg of TiO_2 were also blended in the chitosan solution (1% w/v) to obtain mAL/CH/TiO_2. The beads were collected, washed, and dried in an oven at 60°C before the use.

2.3 UV-Visible measurements.

UV-Vis spectra were recorded using a Varian CARY 5 UV-Vis-NIR spectrophotometer (Varian Inc., now Agilent Technologies Inc., Santa Clara, CA, USA). Spectra were collected in a 200–800 nm range, at a 1 nm/s scan rate, and the TC amounts were monitored by measuring the absorbance intensity at λ=358 nm. More specifically, since the matrix effect, the method of the standard addition was used to infer the exact TC concentration when mAL/CH (or mAL/CH/TiO_2) were used.

2.4 Scanning Electron Microscopy (SEM).

In the case of SEM analysis, an electron microscope FESEM-EDX Carl Zeiss Sigma 300 VP was used. The samples were fixed on aluminum stubs and then sputtered with graphite using a Sputter Quorum Q150. Additionally, the chemical composition was determined by EDX under the scanning electron microscope and X-rays diffraction.

2.5 *In batch* equilibrium experiments.

Experiments were carried out to study the behavior of the various adsorbents respect to the TC adsorption onto mAL/CH, with and without TiO_2 (mAL/CH/TiO_2).

The adsorption capacities were calculated in terms of q_t (mg×g^{-1}) at time t for TC, by applying the following **Equation 1** (Rizzi et al., 2019a, 2019b):

$$q_t = \frac{C_0 - C_t}{W} \times V \quad (1)$$

where V represents the volume of adsorbed solution (15 mL), W is the weight of the dried adsorbent material (g), C_0 and C_t (mg×L^{-1}) represent the concentration of TC at initial and t time.

2.6 *In batch* adsorption experiments.

A fixed amount of adsorbent into flasks containing 15 mL of TC solution at different initial concentrations (1.65×10^{-4}M, 5×10^{-5}M, 2.5×10^{-5}M, corresponding to 79 mg/L, 24 mg/L and 12 mg/L of TC, respectively) was used. The adsorbents were put in flasks containing TC solutions, under continuous stirring at 250 rpm, and UV-Vis absorption spectra were recorded to evaluate the TC removal efficiency from water. To infer the exact TC concentration, the internal standard calibration method was used. The effect of both solution ionic strength, (by using different salts at 0.1 M and 2 M of concentration), and changes in pH values, (ranging from 2 to 12), were also investigated.

Besides, the effect of adsorbent amount was also explored, modifying the adsorbent amount (from 0.25 g to 2.00 g).

2.7 *In batch* desorption experiments.

After the TC adsorption from water, the adsorbent was taken in contact with solutions having high ionic strength. $MgCl_2$ 2 M was selected as the best salt to be able to induce the release of the adsorbed TC. With the same approach adopted for the adsorption of TC, the UV-Vis investigation was used to assess the amount of the desorbed pollutant.

In detail, after the TC adsorption the adsorbent was washed with fresh water to remove the not adsorbed TC and swollen in the solution for the release. It is worth to mention that in $MgCl_2$ the following molar absorption coefficients (ε) was used: 17200 M^{-1} cm^{-1}.

2.8 Adsorption kinetics.

In order to obtain information related to the kinetics of the adsorption process, both pseudo-first-order (PFO) and pseudo-second-order (PSO) kinetic models were, at first, adopted to experimental data

(Berhane et al., 2017; Rizzi et al., 2019a, 2019b). Specifically, the linearized equations for PFO (**Equation 2**) and PSO (**Equation 3**) models were applied:

$$\mathbf{ln(q_e - q_t) = ln(q_e) - k_1 \times t} \quad (2)$$

$$\mathbf{\frac{t}{q_t} = \frac{1}{k_2 q_{e2}^2} + \frac{1}{q_e} \times t} \quad (3)$$

where q_e and q_t represent the adsorption capacities at equilibrium and at time t, respectively ($mg \times g^{-1}$) and k_1 (min^{-1}) and k_2 ($L \times (mg \times min)^{-1}$) are the rate constants of PFO and PSO models, respectively. It is worth to mention that the k_1 and k_2 parameters may or may not be dependent on the initial concentration of the solute or other factors (Berhane et al., 2017), and PFO and PSO models could be not enough to describe the global adsorption processes (Berhane et al., 2017; Tien and Ramarao, 2014).

So, to improve these kinetic investigations and to obtain more information about the adsorption process, the Langmuir kinetic model was also investigated. Starting from the work of Tien and Ramarao (2014) that explained the relation between the Langmuir kinetic and PFO/PSO models, an approach like that used by Berhane et al. (2017) to derivate the Langmuir kinetic constants, from the PFO and PSO models, was herein used.

So, k_1 and k_2 constants can be rearranged as reported in the following discussion (Berhane et al., 2017).

It has been demonstrated that, if the Langmuir equilibrium constant, K_L, (see **Equation 9**) is known from equilibrium batch experiments, the Langmuir kinetic constants can be calculated from PFO and PSO models.

For the PFO one it is possible to assess that:

$$\mathbf{k_d = \frac{k_1}{K_L \times C_0 + 1}} \quad (4)$$

$$\mathbf{k_a = \frac{K_L \times k_1}{K_L \times C_0 + 1}} \quad (5)$$

where k_a is the adsorption rate constant ($L\times(mg\times min)^{-1}$) and k_d is the desorption rate constant (min^{-1}).

Conversely for PSO:

$$\mathbf{k_a} = \frac{-2\mathbf{q_e}\times\mathbf{k_2}}{-\left(\beta+ C_0+\frac{1}{K_L}\right)-\left(\beta^2+ C_0{}^2+\frac{1}{K_L{}^2}-2\beta\times C_0+\frac{2\beta-2C_0}{k_L}\right)^{0.5}} \quad (6)$$

where:

$$\boldsymbol{\beta} = \frac{C_0-C_e}{\frac{q_e}{Q_0}} \quad (7)$$

and Q_0 represents the maximum adsorption capacity calculated from **Equation 9**.

So, knowing k_a from **Equation 6,** k_d can be calculated by using **Equation 8**.

$$\mathbf{K_L} = \frac{K_a}{K_d} \quad (8)$$

For more details about the adopted assumptions and applicability of the Langmuir kinetic model, see the works of Berhane et al. (2017) and Tien and Ramarao (2014).

2.9 Adsorption Isotherms.

Among the reported models, the Langmuir, Freundlich and Temkin isotherm equations were used (Rizzi et al. 2019a, 2019b) to analyze the sorption process of TC on the presented adsorbents. When the Langmuir model well fit the experimental data, it describes the adsorption on homogeneous surfaces with uniformly energetic adsorption sites and monolayer coverage. The interaction between adsorbed molecules is not predicted. **Equation 9** reports the adopted linear form of the Langmuir equation:

$$\frac{C_e}{q_e} = \frac{1}{K_L\,Q_0} + \frac{C_e}{Q_0} \quad (9)$$

where q_e ($mg\times g^{-1}$) is the adsorbed amount of TC at equilibrium, C_e is the equilibrium concentration of the TC ($mg\times L^{-1}$) in solution, K_L is Langmuir equilibrium constant ($L\times mg^{-1}$) and Q_0 the maximum adsorption capacity ($mg\times g^{-1}$). The Freundlich isotherm was also used. The assumption of the model is that the surface of the adsorbent is heterogeneous and adsorption sites having different energy of

adsorption are contemplated. The energy of adsorption varies as a function of the surface coverage. **Equation 10** reports the linear form of this equation.

$$\log(q_e) = \log(K_F) + \frac{1}{n}\log(C_e) \quad (10)$$

where K_F ($L \times mg^{-1}$) is the Freundlich constant and n is the heterogeneity factor. K_F is related to the adsorption capacity, whereas the 1/n value indicates if the isotherm is irreversible (1/n=0), favorable ($0<1/n<1$) or unfavorable ($1/n>1$).

When the Temkin model in its linear form was adopted, the **Equation 11** was adopted.

$$q_e = B_1 ln(K_T) + B_1 ln(C_e) \quad (11)$$

The isotherm constants B_1 and K_T can be determined from the slope and the intercept of **Equation 11**, respectively. K_T is the equilibrium binding constant ($L \times mol^{-1}$) corresponding to the maximum binding energy and B_1 is related to the heat of adsorption. In this case, if the model well fit the experimental data, it indicates that the heat of adsorption during the adsorption process linearly decreases with the coverage due to adsorbent–adsorbate interactions. The adsorption is characterized by a uniform distribution of binding energies.

2.10 Thermodynamic studies.

Free energy (ΔG°), entropy (ΔS°), and enthalpy (ΔH°) were determined (Chen et al., 2016) for the TC adsorption on mAL/CH/TiO_2 at the three selected temperatures, 298, 323 and 333 K. In particular, the change in free energy (ΔG°) was estimated from **Equation 12**:

$$\Delta G° = - RT\, Ln\, K_{eq} \quad (12)$$

in which R is the universal gas constant (8.314 J/mol K), T is the temperature (K) and K_{eq} represents the equilibrium constant. So, the values of ΔH° and ΔS° were inferred combining **Equation 12** with **Equation 13** obtaining **Equation 14**.

$$\Delta G° = \Delta H° - T\Delta S° \quad (13)$$

$$\ln K_{eq} = -\frac{(\Delta H°)}{RT} + \frac{(\Delta S°)}{R} \quad (14)$$

2.11 Photodegradation of TC.

Among several ways to induce the oxidation of the pollutant, the photodegradation of TC was accomplished using UV, H_2O_2 and their synergic use also in presence of Fe^{2+} under Fenton conditions. After the adsorption of TC, the adsorbent blended with TiO_2 was washed with fresh water in order to remove the not adsorbed TC and swollen in 15 mL of water. A UV lamp was used to irradiate the adsorbent (UV fluorescent lamp, Spectroline, Model CNF 280C/FE, λ 254 nm, light flux 0.2 mW/cm^2; USA) adopting several contact times. The percentage of the photodegraded TC was calculated releasing the TC after the irradiation. Knowing the adsorbed TC amount, and the time necessary to desorb completely the TC, the photodegraded TC was inferred as follow (**Equation 15**):

$$\%\ \textbf{of photodegraded TC} = \frac{\textbf{amount of TC adsorbed} - \textbf{amount of TC released}}{\textbf{amount of TC adsorbed}} \times \mathbf{100} \quad (15)$$

UV-Vis spectroscopy was used to calculate the amount reported in **Equation 15**. H_2O_2 was used to trigger the UV light effect at concentration of 1.0×10^{-3}M and 1.0×10^{-2}M. Fe^{2+} for the Fenton reaction, in absence and in presence of UV light, was added as $FeSO_4$ at concentration of 1.0×10^{-5}M. The TC photodegradation after the release in $MgCl_2$ was also evaluated adopting the same conditions of work previously described.

3. RESULTS AND DISCUSSION

The proposed adsorbent was preliminary investigated from the morphological point of view, through microscopic analyses (**Figures S1-S2**), evidencing the adsorbent great roughness (a key feature for adsorbent materials). However, it is worth to mention that the mAL and CH use as adsorbents for pollutant removal is not new; indeed, these materials were already used for removing textile dyes from water (Semeraro et al., 2017). The novelty lies in the realization of a composite adsorbent material obtained by covering the alginate beads with chitosan and by enriching them with TiO_2 for environmental applications. In particular, in perspective of performing a more eco-sustainable strategy to remove emerging pollutants from water (Belayutham et al., 2016), the attention was mainly focused on the TC removal from water by studying the parameters affecting its adsorption.

This composite material resulted very effective in removing TC, and as alternative to the removal and recycling of the TC, its photodegradation was also proposed by adding TiO_2 P25 in order to exploit its photocatalytic properties. About this, in **Figures S2** the Energy dispersive X-ray analysis is reported and it indicated a quite homogeneous distribution of TiO_2 in the sorbent beads.

3.1 TC adsorption onto mAL/CH and mAL/CH/TiO_2.

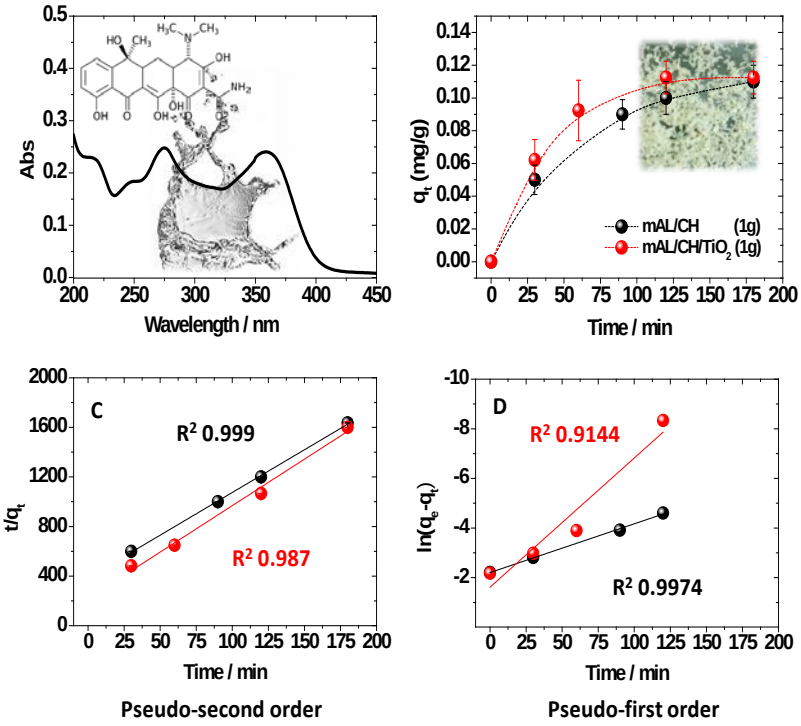

Figure 1: *UV-Vis absorption spectrum of TC in water, 2.50×10^{-5}M at pH 6, and its chemical structure* ***(A)****; comparison between the q_t values related to 1.00g of mAL/CH and mAL/CH/TiO_2 swollen in a neutral TC solution 2.50×10^{-5}M* ***(B)****; Pseudo-second* ***(C)*** *and pseudo-first* ***(D)*** *order kinetic models applied to the experimental data reported in the panel B.*

TC (molecular structure in the inset of **Figure 1A**) exhibits a characteristic UV-Vis absorption spectrum with two main absorption bands in the UV region at 275 nm and 360 nm, respectively. These bands correspond to a $\pi\rightarrow\pi^*$ transitions (Abdel-Ghani et al., 2016; Abdulghani et al., 2013) and are strongly affected by the pH and ionic strength of the aqueous solution (Moussavi and Khosravi, 2011).

During this work the TC spectroscopic features were considered diagnostic to follow the TC removal from water and to calculate the adsorption capacities of the proposed adsorbent. So, in **Figure 1B**,

the adsorption capacities of mAL/CH/TiO_2 at several contact time (**Equation 1**), and the comparison with mAL/CH to check possible differences between mAL/CH/TiO_2 and mAL/CH, are reported. In both cases, by swelling 1.00 g of adsorbent in 15 mL of aqueous TC solution at 2.50×10^{-5}M, a significant TC removal was observed: after 180 minutes, about the 50% of pollutant resulted removed. As reported in **Figure 1B**, the amount of the adsorbed TC, and thus the q_t values, increased at the increasing of the contact time, reaching a plateau after 120 minutes.

Specifically, the high concentration gradient of the adsorbate between the solution and the adsorbent surface, resulted in a TC fast transfer onto the solid surface (Fan et al., 2016). At the beginning, the presence of a large quantity of free sites available for the TC adsorption onto the mAL/CH surface increased the q_t values, but with elapsing the contact time, the free sites decreased, and the TC relative adsorption was reduced reaching a plateau. Moreover, as already observed in the work of Chen et al. (2016), the finding can be explained considering that the adsorbed TC molecules could repel the TC molecules in solution due to the arising of repulsive forces, hindering the further diffusion of TC molecules into the adsorbent structure (Chen et al., 2016). The good performance of the adsorbent, suggested to investigate the behavior of the single components, chitosan powder and alginate beads without the chitosan external layer, to assess the synergy of the composite material. The results (**Figure S3**) clearly showed the incapacity of the single materials to adsorb TC.

More detailed information were inferred performing the kinetic analysis by using **Equations 2** and **3**. The obtained R^2 values indicated as the PSO model (**Figure 1C**) better fitted the experimental data for both the adsorbents if compared with results obtained from the PFO model **(Figure 1D)**. The calculated adsorption capacity values ($q_{e,calc}$) cannot match their experimental values ($q_{e,exp}$ ~ 0.12 mg/g) nicely when the PFO model was used ($q_{e,calc}$: 0.06 mg/g for mAL/CH/TiO_2 and 0.025 mg/g for mAL/CH).

In fact, the PFO model offers a simplified approach and usually cannot be used to describe complicated kinetic mechanism of adsorption involving more than one type of rate-limiting processes (Berhane et al., 2017).

From the kinetic analysis, the following kinetic constants, k_2, were obtained: 0.12 ($L\times(mg\times min)^{-1}$) and 0.25 ($L\times(mg\times min)^{-1}$) for mAL/CH and mAL/CH/$TiO_2$, respectively. So, the mAL/CH system modified by adding TiO_2 (mAL/CH/TiO_2) showed a quite similar behavior, with mAL/CH/TiO_2 that occurred slightly more efficient (red line in **Figure 1B**). For that reason and for the presence of TiO_2, used to photodegrade the EP, mAL/CH/TiO_2 system was selected as the most suitable adsorbent for our purpose and it was further characterized by changing the experimental conditions of work, such as the amount of adsorbent and adsorbate, the temperature values and the pH of the solutions.

3.1.1 Effect of pH

An overview about the percentage of TC removal under different experimental conditions is reported in **Figure 2**. Starting from the pH role, the TC removal percentages at neutral, acid and basic pH values (at room temperature) were considered. The molecular structure of TC has three dissociation constants: at pH < 3.3, TC exists in the cationic form (TCH_3^+) with pK_{a_1}=3.3; in the range 3.3–7.7, the main form is the zwitterion ($TCH_2^{\pm}$) with pK_{a_2}=7.7; and at pH > 7.7 is in the two anionic forms, TCH^- and TC^{2-}, characterized by pK_{a_3}=9.7 (**Figure S4A**) (Chen et al., 2016; Dong et al., 2018). Since the solution pH values affected the main TC functional groups, the UV-Vis absorption bands changed accordingly (**Figure S4B**). For this reason, the TC adsorption onto mAL/CH/TiO_2, at 298 K, was investigated at pH 2, pH 6 and pH 12 in which the main TCH_3^+, $TCH_2^{\pm}$ and TC_2^- forms occurred, respectively. Interestingly, by comparing the removal percentage with neutral and acid condition, at pH 12, the removal of TC appeared more favored. ~80% of TC was removed (**Figure 2A**), obtaining a q_t value (**Figure S5**) similar to the theoretical one, which corresponds to an almost complete TC removal (q_{max} = 0.18 mg/L). These findings can be explained by considering that the solution pH affected both the TC and chitosan charges influencing the interaction between them (Caroni et al., 2009; Chen et al., 2016; Shao et al., 2012). Indeed, the chitosan pH_{PZC} ranges from 6 to 7 (Lee et al., 2013), therefore below pH 6-7, chitosan and TCH_3^+ were protonated and positive charged indicating that pure electrostatic interactions cannot arise. On the other hand, above to neutral

335 condition of work, the chitosan amino groups were mainly deprotonated and again pure electrostatic
336 interaction with TC^{2-} cannot occur. Based on these considerations, as suggested by the adsorption
337 capacities observed at all pH conditions of work, H-bonds and Wan der Waals forces between
338 deprotonated chitosan and the TC oxygen atoms were the most important involved interactions.
339 However, the complete absence of electrostatic interaction cannot be ruled out, because also when
340 the TC was in the zwitterionic form ($TCH_2^{\pm}$), the removal percentage was high.
341 According to the literature, probably the mechanism of adsorption involved a chitosan chains
342 rearrangement, due to the break of the inter- and intrachain interactions during the chitosan
343 protonation and deprotonation processes, restituting an increase in water clusters within the particles,
344 making the structure more porous (Caroni et al., 2009).

345

346 *3.1.2 Effect of temperature.*

347 By a thermodynamic point of view, the process had an endothermic character (Chen et al., 2016).
348 Indeed, increasing the temperature values from 298 to 333 K, the TC removal increased (**Figure 2A**).
349 By using **Equations 12-14**, the following thermodynamic parameters were obtained: $\Delta G°_{298K}$=-6.70
350 KJ/mol and $\Delta H°$=+40.00 KJ/mol, indicating the spontaneous and endothermic character of this
351 process, respectively (see also **Figure S6** and **Table S1**). The positive $\Delta S°$=+155.00 J/mol×K
352 suggested that, at the adsorbent–adsorbate interface during the adsorption process, the randomness
353 increased (Chen et al., 2016).

354

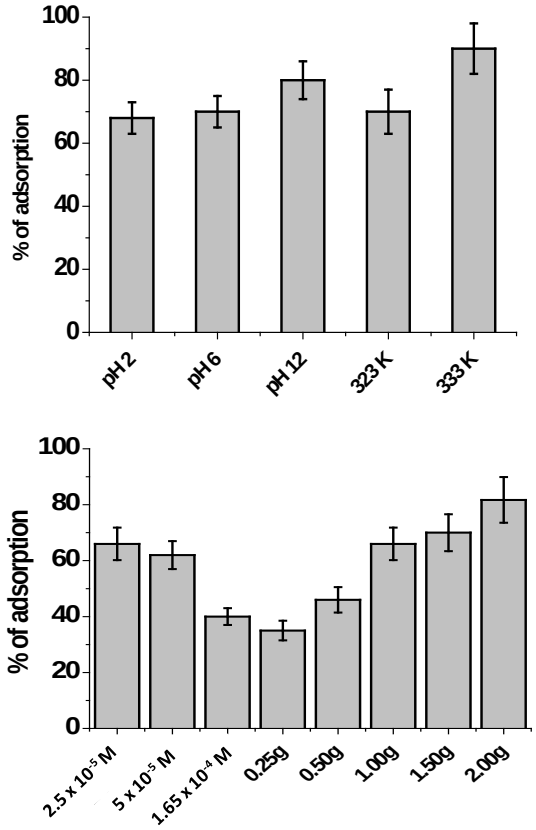

Figure 2: *% of TC adsorption (from TC solution 2.50×10^{-5}M at pH 6) on 1.00g of mAL/CH and mAL/CH/TiO_2 specifically evaluating the effect of pH and temperature values during the adsorption on mAL/CH/TiO_2 (**A**); % of TC adsorption on 1.00g of mAL/CH/TiO_2 evaluating the effect of TC and adsorbent amount (pH 6) (**B**).*

3.1.3 Effect of the TC concentration and adsorbent amount.

Regarding the adsorbent amount role, by increasing the mAL/CH/TiO_2 quantity from 0.25 g to 2.00 g, the TC adsorption percentage increased from about 40% to 90% at the same contact time, indicating that more free sites were available on the adsorbents for hosting TC (**Figure 2B**) (Rizzi et al., 2019a, 2019b). On the other hand, the adsorption capacities, by increasing the amount of the adsorbent, decreased (**Figure S7A**). This can be explained considering that, by using a large amount of adsorbent, the adsorption sites remained unsaturated during the process, reducing on a whole the q_t values. Interestingly, by increasing the TC concentration (**Figure 2B**), from 2.50×10^{-5}M to 1.65×10^{-4}M, the removal efficiency decreased, from 60% to 40%, but the adsorption capacity (q_e) increased, from 0.11 to 0.45 mg/g (**Figure S8A**). This result indicated that a high TC concentration in solution determined a greater concentration gradient between the aqueous solution and mAL/CH/TiO_2 surface incrementing the driving force of the adsorption that favored the mass transfer of TC from the aqueous solution to the adsorbent particles surface, resulting in higher TC adsorption capacity (Chen et al., 2016; Gunay et al., 2007; Rizzi et al., 2019a, 2019b).

To understand better this behavior and to infer information about the controlling mechanisms involved during the adsorption process, kinetic models were applied (Berhane et al., 2017; Shahmohammadi-Kalalagh et al., 2011; Tien and Ramarao, 2014). In this case, due to the results regarding the influence of TC concentration and adsorbent amount, as first step the PSO model was applied (**Figures S7B,C** and **S8B**), obtaining the following kinetic constants: 0.07 ($L\times(mg\times min)^{-1}$), 0.25 ($L\times(mg\times min)^{-1}$), 0.60 ($L\times(mg\times min)^{-1}$), 0.65 ($L\times(mg\times min)^{-1}$) and 0.95 ($L\times(mg\times min)^{-1}$) from 0.25 to 2.00 g of adsorbent, respectively. While, applying again the PSO model, for more concentrated and diluted TC solution, the following kinetic constant values were inferred: 0.2 ($L\times(mg\times min)^{-1}$) and 0.25 ($L\times(mg\times min)^{-1}$), respectively (**Figure S8B**). However, k_2 parameters from the PSO model could be dependent on experimental conditions of work, *i.e.* from the TC concentration in solution that changes during the experiment (Berhane et al., 2017). Further, Regazzoni (2020) explains that the use of the PSO model could be suitable for describing the whole adsorption process and inferring kinetic

information if the initial concentration (C_0) of the pollutant is low. For these reasons, to gain more information about the mechanism of the adsorption, the obtained findings were converted, as second step, to the Langmuir kinetic model PSO-derived. By using **Equations 6** and **8**, the k_a and k_d values were calculated, in the range of the adopted conditions of work, and occurred ≈ 0.001 ($L\times(mg\times min)^{-1}$) and 0.0004 min^{-1}, respectively.

Subsequently, following the approach of Berhane et al. (2017) the term $\lambda \times t$ was calculated ($\boldsymbol{\lambda} = \sqrt{\boldsymbol{K_a^2} \times (\boldsymbol{\beta} + \boldsymbol{C_0} + \frac{\mathbf{1}}{\boldsymbol{k_L}})^2 - \mathbf{4}\boldsymbol{K_a^2}\boldsymbol{\beta}\boldsymbol{C_0}}$). The Authors report that the Langmuir kinetic model reduces to PSO one only when certain conditions are satisfied, *i.e.* when $\lambda \times t$ is small. In particular, the Authors explain that a $\lambda \times t \approx 0.50$ produces an error of about 10% and, in our case, $\lambda \times t$ exceeded 0.50 after only 30 min. So, to infer more corrected kinetic constant values, as described by Berhane et al. (2017), a numerical model should be used for adjusting the values of the calculated k_a and k_d. Consequently, the adsorption of TC was complex and beside the diffusion role, mainly predicted by PSO, other factors should be taken in consideration. In fact, an inherent assumption with the adopted approach is that the Langmuir equilibrium isotherm was the proper model (Berhane et al., 2017). On the other hand, as will be discussed in the next paragraph, it was not possible during this study to predict a single isotherm model, as the Langmuir one, to describe the process. Indeed, under our experimental conditions of work, the Freundlich and Temkin isotherms well fitted also the experimental data; as consequence, the only use of the K_L (and also the value of the maximum adsorption capacity, Q_0, should affect the results obtaining during the Langmuir kinetic investigation) cannot take into account the global mechanism of adsorption (for example, the assumptions of other isotherms are not considered).

Overall, by considering again the work of Berhane et al. (2017), the obtained kinetic findings can be rationalized considering that during the adsorption process, among the possible factors that could be considered, the intraparticle-diffusion (IPD) played a key role. Probably, the surface adsorption of

TC was dominant at the beginning of the process and the IPD became the rate-limiting process extending the contact times (Berhane et al., 2017).

So, our results, that implied the role of TC amount and free active sites available for the adsorption, can be used in conjunction with a mass-transport model to detail the TC transport through the adsorbent (Berhane et al., 2017)

To confirm the IPD role, the Weber-Morris model was thus applied (Chen et al., 2016). Through the Weber equation ($q_t=K_i t^{1/2}$), the kinetic constant related to the intra-particle diffusion rate in mg/(g×min$^{0.5}$) can be calculated from the slope of the q_t vs $t^{1/2}$ plot. If multiple linear segments are necessary to fit the experimental data, as happens in **Figure 3A**, then two or more steps may be involved in the adsorption process. Practically, under our experimental conditions, the TC adsorption process was constituted by two main sequential phenomena: the initial TC diffusion from the solution to the external surface of the adsorbent was followed by a second step corresponding to the intra-particle adsorption and diffusion (Berhane et al., 2017; Fan et al., 2016). Additionally, **Figure 3A** indicates that, at higher TC concentration, the time period during which the IPD was the adsorption rate limiting factor was longer occurring with a higher contribute (Moussavi and Khosravi, 2011). Probably, at the beginning of the process, the favored mass transfer leveled off the effect of the TC diffusion towards the beads surface, and the limiting step was the diffusion inside the pores (hindered by the adsorbed molecules). Accordingly, by fixing the TC concentration at 2.50×10^{-5}M and changing the adsorbent amount, the Weber plot reported in **Figure 3B** shows once again the presence of multiple steps during the adsorption process, especially evident when reducing the amount of the adsorbent revealing the contribute of IPD. Conversely, when the adsorbent was in excess, the intra-particle diffusion tended to level off, and the diffusion of TC from the bulk of the solution on the surface of the adsorbent controlled the adsorption process.

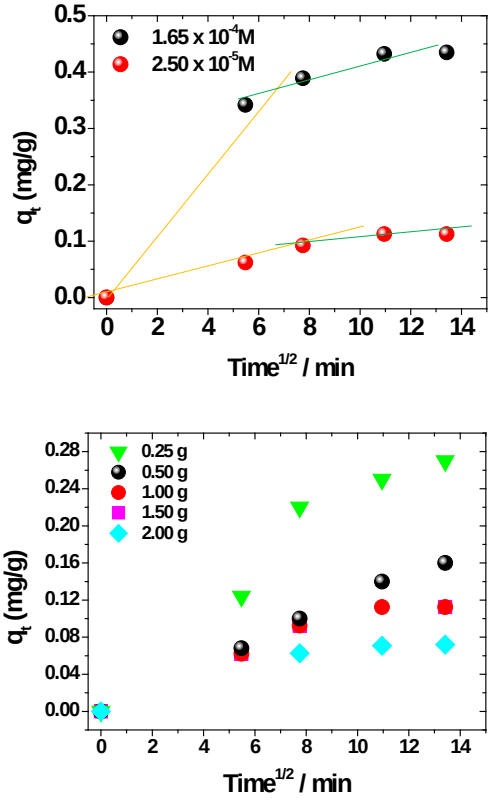

Figure 3: *Weber-Morris plot using mAL/CH/TiO₂ varying the amount of TC and fixing at 1.00g the amount of the adsorbent (**A**) and viceversa fixing the TC at 2.50×10⁻⁵M (pH 6) and varying the adsorbent amount (**B**).*

428

429 *3.1.4 Isotherms of adsorption.*

430 The equilibrium adsorption isotherms are important for better understanding the adsorption
431 relationship between TC and the adsorbent surface (Chen et al., 2016; El Haddad et al., 2013; Fan et
432 al., 2016; Zhu et al, 2018). In particular, experimental data were analyzed according to the Langmuir,
433 Freundlich, and Temkin models, by fitting the data with **Equations 9, 10** and **11**, in order to select
434 the most appropriate model for the studied adsorption process. In detail, the concentration of neutral

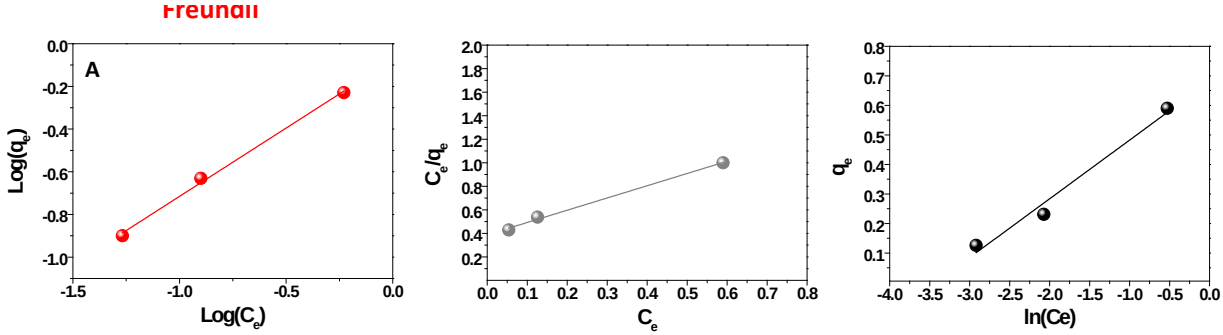

Figure 4: *Isotherms of adsorption when mAL/CH/TiO₂ are used*

TC solutions was changed in the range 2.50×10^{-5}M - 1.65×10^{-4}M (0.18 mg/15 mL-1.18 mg/15 mL) and mAL/CH/TiO_2 were swollen inside. For inferring the q_e and C_e values for each experiment, the adsorption equilibrium was attained.

As it is possible to observe in **Figure 4**, in accordance with the obtained R^2 values, both Langmuir and Freundlich models well fitted the experimental data, while the Temkin model presented a slightly lower R^2 value. **Table 1** reports the calculated isotherm parameters.

Freundlich Isotherm Model			**Langmuir Isotherm Model**			**Temkin Isotherm Model**		
K_F (L×mg^{-1})	n	R^2	K_L (L×mg^{-1})	Q_0 (mg×g^{-1})	R^2	K_T (L×mol^{-1})	B_1	R^2
0.85	1.6	0.9986	2.74	0.96	0.9983	30	0.2	0.9613

Table 1: *Isotherm parameters for the adsorption of TC onto mAL/CH/TiO_2*

The applicability of three isotherms on the adsorption of TC onto mAL/CH/TiO_2 suggests that the process occurred onto heterogeneous surfaces (Guler and Sarioglu, 2014) with a complex mechanism of adsorption considering the previous kinetic considerations. It means that it was not possible to describe the adsorption process by using a single isotherm model (Rizzi et al., 2019a, 2019b). Further, the *n* value, indicated in the Freundlich equation, represents the adsorption strength and, as suggested by Chen et al. (2016), if this value ranged from 1 to 10, it indicates that the adsorption process is favored. Indeed, in our case a *n* value of 1.6 was obtained. As for the Langmuir parameters, a K_L value of 2.74 L·mg^{-1} and a Q_0 of 0.96 mg/g (maximum adsorption capacity) were obtained.

3.2 Recycle of the adsorbent and adsorbate

In the perspective of applying the principles of the "Cleaner technologies", the recycle of adsorbent and adsorbate should be considered one of the most important properties for environmental

applications. Indeed, the recovery of micro-sized hydrogel from solution by means of desorption process, is one of the main challenges, together with the possibility of selectively removing and recovering also targeted pollutants (Thakur et al., 2018). So, the study was continued evaluating both the TC desorption and the combined effect of adsorption-photodegradation of TC via advanced oxidation processes, as an alternative method for the treatment of organic polluted wastewater.

3.2.1 Release of TC.

First of all, the possibility of releasing TC from mAL/CH/TiO_2 was investigated, stirring the microbeads previously loaded with TC in different organic solvents or in aqueous solution changing the pH values (Shao et al., 2012). However, the use of different organic solvents did not allow any desorption (*data not shown*). Further, considering the results relative to the TC adsorption at various solution pHs (**Figure 2A**), it is clear as the TC desorption did not occur under these experimental conditions, confirming the slight role of electrostatic forces. Instead, when the beads were swollen in a fresh aqueous solution (15 mL) at a different ionic strength, interesting results were observed. More specifically, the following salts, at different concentrations, were adopted: NaCl, LiCl, $CaCl_2$, $MgSO_4$ and $MgCl_2$. In **Figure 5**, as an example, the release obtained in $MgCl_2$ (2M) solution from mAL/CH and mAL/CH/TiO_2 (**Figure 5A**), after the TC adsorption, and a comparison between the release

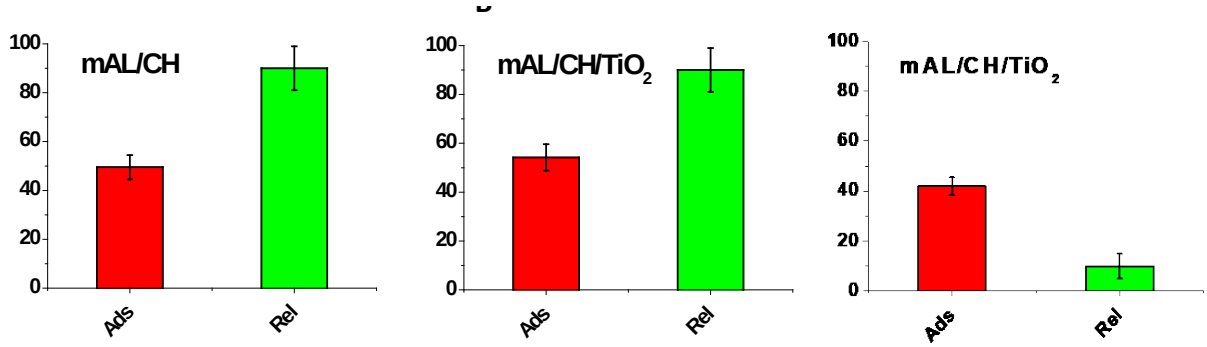

Figure 5: *% of TC adsorption (from a TC solution 2.50 ×10^{-5}M at pH 6) and release in $MgCl_2$ by using mAL/CH (**A**) and mAL/CH/TiO_2 (**B**); and in NaCl by using mAL/CH/TiO_2 (**D**). The contact time of adsorption and desorption is indicated.*

obtained in presence of $MgCl_2$ 2M (**Figure 5B**) and NaCl 2M (**Figure 5C**) from mAL/CH/TiO_2 are reported.

It is evident that the addition of Mg-based salts at high concentration (2 M) resulted more suitable, allowing the release of almost the 100% of the adsorbed TC (**Figure 5B**), suggesting a potential cleaner reuse of the pollutant. Further, with the aim of showing the better performance of the adsorbent enriched with TiO_2, in **Figures 5A** and **5B**, a comparison between the time needed for TC releasing in presence (mAL/CH/TiO_2) and in absence of TiO_2 (mAL/CH) is made.

In detail, in **Figures 5A, B**, analyzing the percentage of the TC released in 2M $MgCl_2$ solution, it is possible to observe that 2h were necessary to completely desorb the TC from mAL/CH, while, in the case of mAL/CH/TiO_2, the same result was achieved after only 1h, confirming the better performance of this adsorbent. These findings can be explained considering the polymeric network of the mAL/CH/TiO_2 beads. Indeed, Ca^{2+} is necessary for crosslinking the alginate chains, enabling the microbeads formation (Semeraro et al., 2017); so, the use of other bivalent cations, as Mg^{2+}, different from Ca^{2+}, broke these structures favoring the TC release preventing the adsorbent reuse. In particular, as discussed in Pakdel and Peighambardoust (2018), the charges in a network of a polyelectrolytic hydrogel determines a difference of osmotic pressure between the gel phase and the aqueous phase, that is the driving force inducing the swelling of the material until the pressure difference gets zero. Therefore, changing the ionic strength by increasing the free counter ions concentration, the pressure difference should be enhanced leading to a higher swelling of the gel (Pakdel and Peighambardoust, 2018). Further, TC is also able to complex bivalent ions, forming chelates through its keto-enolate moiety, that could be thus involved during the desorption process (Lopez-Penalver et al., 2010). Consequently, by changing the solution ionic strength adding a Mg^{2+}-based salt, it was possible to recover the pollutant, but the adsorbent cannot be recycled due to the swelling and breaking of three-dimensional microbeads network.

3.2.2 Photocatalytic degradation of TC: Reuse of the adsorbent mAL/CH/TiO_2

The adsorbent reuse could be gained by photodegrading the adsorbed EP, exploiting the photocatalytic features of the TiO_2 blended inside the chitosan network.

About this aspect, it is worth to mention that the photodegradation of TC is a well-known process for several years and interesting information are reported in literature (Jiang et al., 2018; López-Peñalver et al., 2010). In this paper, the TC degradation was accomplished by means of AOPs. In particular,

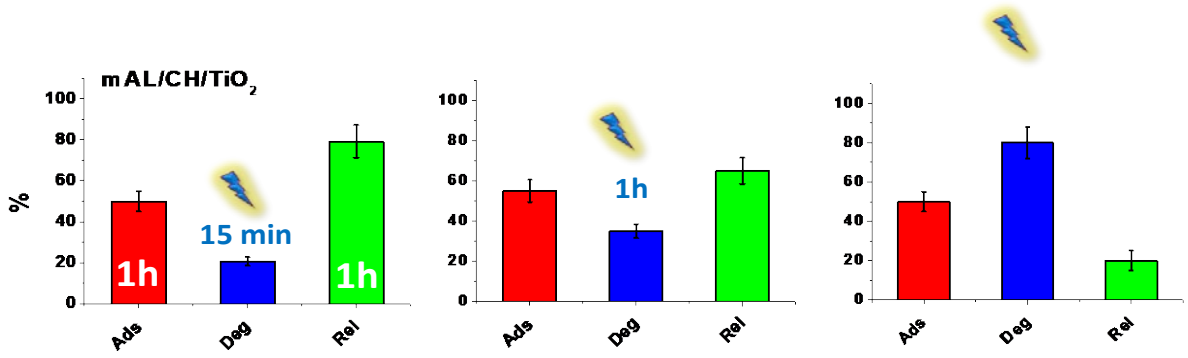

Figure 6: *% of TC adsorption (from a TC solution 2.50×10^{-5}M at pH 6), release in $MgCl_2$, and photodegradation with UV light, by using mAL/CH/TiO_2. The time adopted for the UV light irradiation is reported: 15 min (**A**), 1h (**B**) and 2h (**C**).*

to induce the formation of the hydroxyl radical (•OH) in water (Jiang et al., 2018), the attention was focused on the synergic use of UV, H_2O_2, and Fe(II), through the following combinations: UV-TiO_2, UV/H_2O_2/TiO_2, UV/H_2O_2/Fe/TiO_2. As indicated by Vega et al. (2018), •OH is one of the most important radical species produced by AOPs, being highly reactive and non-selective, with high organic reaction rate constants (Vega and Valdes, 2018).

Starting form the effect of TiO_2 and UV light, in **Figure 6** the percentages of the adsorbed (*Ads*) and photodegraded (*Deg*) TC are reported. The results are compared with the percentage of released TC, chosen as an indirect control. The photodegraded percentage was calculated by using **Equation 15**.

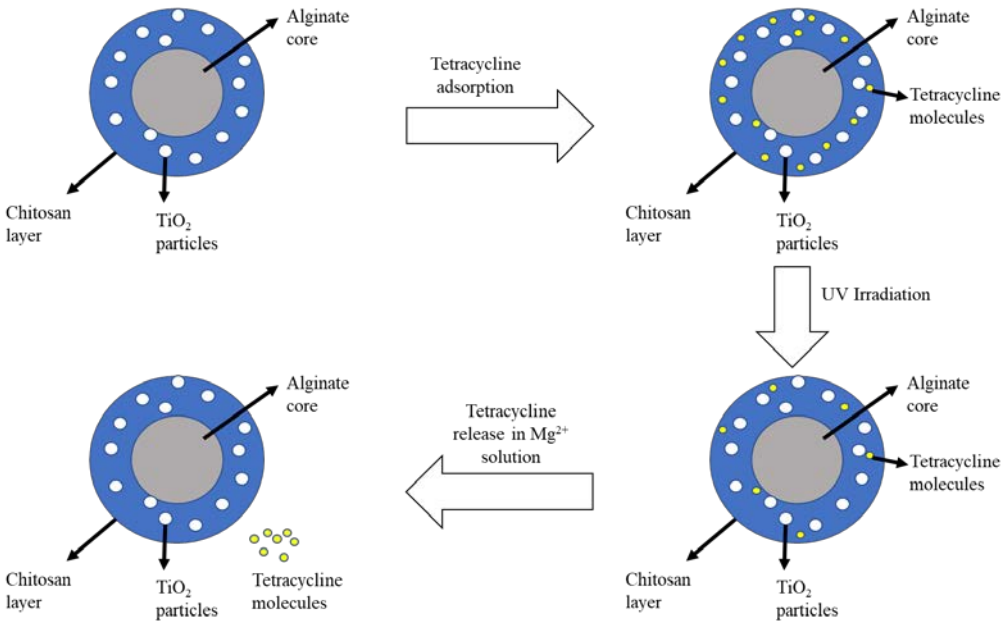

Scheme 1: *Detailed scheme of the procedure adopted to evaluate the TC photodegradation.*

In detail (see **Scheme 1**), fixing 1h as contact time necessary to adsorb the 50% of TC (2.50×10^{-5}M), after the TC adsorption three solution containing mAL/CH/TiO_2 were moderately stirred in 15 mL of fresh water and irradiated with a UV lamp at 254 nm for 15 minutes (**Figure 6A**), 1h (**Figure 6B**) and 2h (**Figure 6C**); after the irradiation, the solution ionic strength was changed by adding $MgCl_2$ to induce the release of the residual TC. In particular, 1h was chosen as suitable contact time to obtain the maximum TC desorption, in a Mg-based solution (2M). The percentage of photodegraded TC was evaluated considering the total amount of adsorbed TC as 100% and subtracting from this number the percentage of released TC, estimated by UV-Vis absorption spectra. As arise from **Figures 6** the TC degradation was UV-dose dependent, and 2h were enough to photodegrade almost the 100% of the adsorbed TC. These results suggested the possibility to perform cycles of adsorption and degradation to obtain the adsorbent recycle. For that reason, in order to evidence the high performances of mAL/CH/TiO_2, in **Figures 7**, experiments related to cycles of adsorption (indicating as Ads 1, 2 and 3), followed by the photodegradation, are reported.

In particular in **Figure 7A**, after the first cycle of adsorption (*Ads1*), the beads were photodegraded for 2h (adopted as suitable condition of irradiation) and then were once again placed in contact for 1h with a fresh TC solution at a concentration of 2.50×10^{-5}M. Surprisingly, at the same condition of

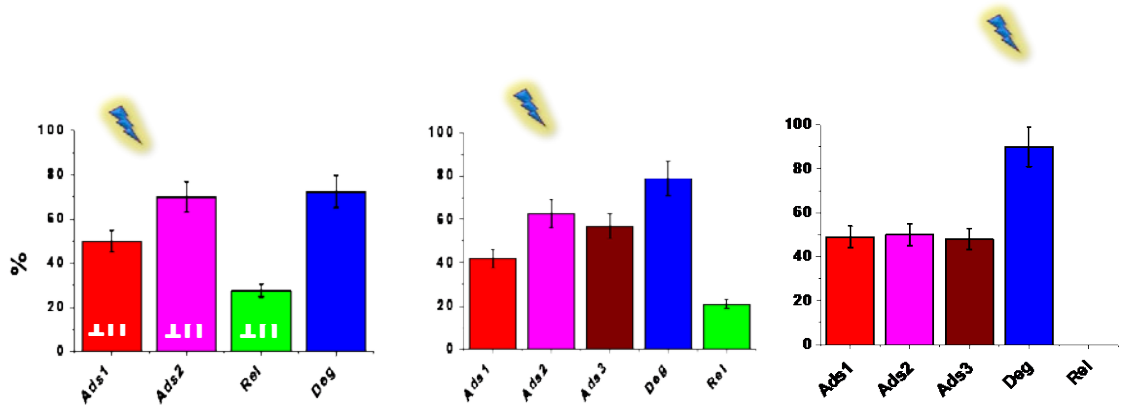

Figure 7: *% of TC adsorption (from a TC solution 2.50×10^{-5}M at pH 6), release in $MgCl_2$, and photodegradation with UV light, by using mAL/CH/TiO_2. The time adopted during the experiments are indicated. TC is adsorbed (Ads1) and photodegraded, then the same beads are used to adsorb again TC (Ads2) and photodegraded (deg) and released (rel) (**A**); the same approach is used for three cycle of adsorption (**B**); three consecutive cycle of TC adsorption followed by the photodegradation for 4h (**C**).*

work used for the first cycle (*Ads1*), the second one (*Ads2*) resulted more efficient, being able of adsorbing about the 80% of the TC from water. This finding could be justified observing the SEM images related to mAL/CH/TiO_2, registered after the first cycle of adsorption and photodegradation, reported in **Figure 8**.

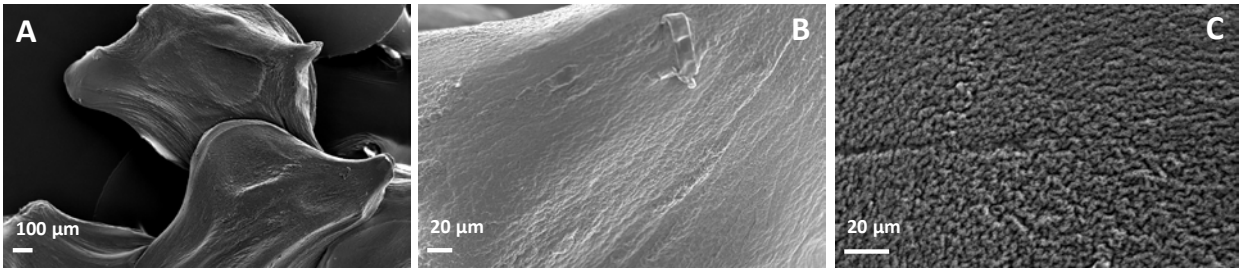

Figure 8: *SEM images of mAL/CH/TiO_2 at different magnification ratio after the TC adsorption and photodegradation.*

The morphology of the beads appears rougher than that (**Figure S1)** related to the microbeads before the adsorption and photodegradation. This can be ascribed to the structural changes of the chitosan outer layer due to the chitosan photochemical oxidation by AOPs. In particular, as reported by Nawi et al. (2011) and Liu et al. (2018), chitosan polymer in presence of •OH radicals (derived both from an irradiated TiO_2 surface and UV irradiation in aqueous environment) can be readily attacked at

carbon atoms of the glucopyranoside ring (being all position equivalent toward the highly reactive •OH radicals), forming a carbonyl group (position C-5 of the pyranose ring) at the end of the radical cascade reactions, without breaking the glycosidic bond and excessively altering the whole polymeric chemical structure (Nawi et al., 2011). However, after the irradiation, chitosan showed a more porous surface morphology (**Figure 8**) probably due to the formation of this carbonyl moiety on the pyranose ring that induced a rearrangement of the polymer chains (Liu et al., 2018; Nawi et al., 2011).

At the end of these experiments, the beads were swollen in a solution having a high ionic strength ($MgCl_2$ 2M) obtaining the amount of the photodegraded TC (**Figure 7A**). Subsequently, the effect of the 3th cycles (*Ads 3*) of adsorption/photodegradation was investigated (**Figure 7B**). Once again, the efficiency of adsorption was very high, with interesting results about the degradation of the adsorbed pollutant that was almost completely degraded. Further, other experiments were performed absorbing consecutively the pollutant from water for 3 cycles (Ads 1, 2 and 3), as reported in **Figure 7C**. In this case, only at the end of the third cycle of adsorption, the photodegradation was attempted. Interestingly, without the UV light irradiation between each cycle, the efficiency of the TC removal occurred to be the same for 3 consecutive cycles (~50% for single adsorption cycle). This finding clearly suggests the key role of the UV irradiation in the beads morphological changes that affected the TC removal percentage. In this latter case, in order to induce a quite complete TC photodegradation, the UV light was used for 4h (**Figure 7C**). As second step, with the aim to reduce the time necessary to photodegrade the pollutant blocked inside the beads, H_2O_2 was used during the photodegradation (López-Peñalver et al., 2010). The experiments were conducted as previously described, but in presence of different amount of hydrogen peroxide, *i.e.* 1.0×10^{-3}M (**Figure 9A**) and 1.0×10^{-2}M (**Figures 9B, C**). It is worth to mention that, under our experimental conditions, the degradation of TC did not occur using H_2O_2 in absence of UV light. On the other hand, fixing the amount of H_2O_2 at 1.0×10^{-2}M (**Figures 9B, C**), the synergic use of UV and H_2O_2 enhanced the oxidation processes and TC was destroyed in 15 minutes. In particular, the UV dose was increased by extending the contact time from 15 minutes to 1h (**Figure 9C**), evidencing as the degradation was

quite complete. Safari et al. (2015) and references therein, suggested that the addition of H_2O_2 to TiO_2 improves the TC degradation. Indeed, additional •OH are produced under this condition due to the photolysis of the peroxidic bond (–O–O–). Finally, experiments were performed also under Fenton conditions with and without UV; however, if free TC in aqueous solution was degraded, on the other hand when adsorbed onto beads the molecules was not destroyed. The following conditions of work were adopted: $FeSO_4$ from 10^{-5}M to 10^{-3}M and H_2O_2 from 10^{-4}M to 10^{-3}M. When UV light was used, 1h was chosen as contact time. Probably the formation of the hydroxyl radical occurred in solution far away from adsorbed TC, and it was rapidly quenched by water.

3.3 Comparison between the Q_{max} values obtained from literature and this work

Table 2 reports the comparison between the Q_{max} values (the maximum adsorption capacity) related to adsorbents, studied to remove TC from water (Dai et al., 2019; Dehghan et al., 2019; Fan et al., 2016; Gao et al., 2012; Liu et al., 2012; Ma et al., 2017; Oladoja et al., 2014; Qin et al., 2018; Raeiatbin and Açıkel, 2017; Shao et al., 2012; Yeşilova et al., 2018; Zhang et al., 2015), and the results observed during this work. It is worth to mention that, in the most cases, different temperature

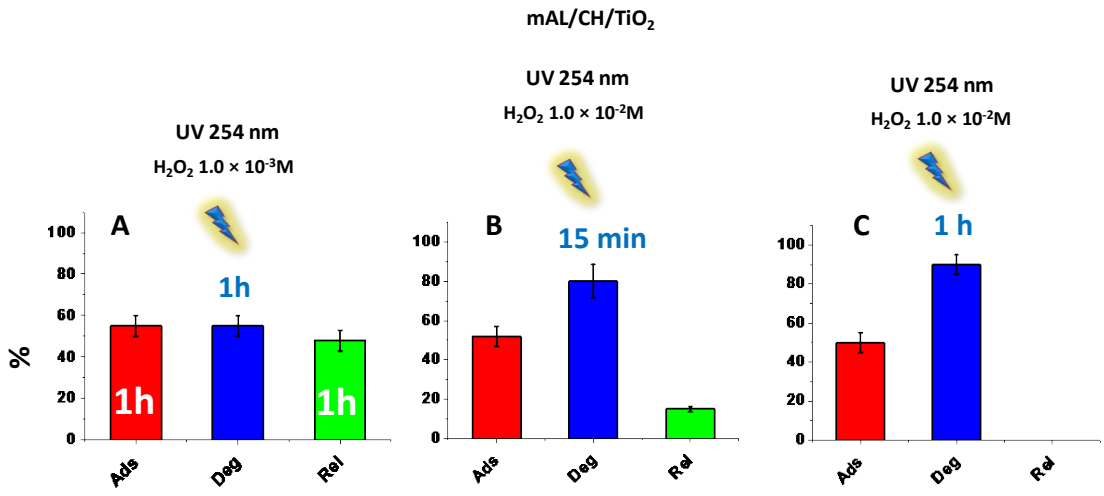

Figure 9: *% of TC adsorption (from a TC solution 2.50 ×10^{-5}M at pH 6), release in $MgCl_2$, and photodegradation with UV light and H_2O_2 1.0 × 10^{-3}M (**A**), 1.0 × 10^{-2}M (**B**) 1.0 × 10^{-2}M (**C**), by using mAL/CH/TiO_2. The time adopted for each experiment is reported.*

and pH values, and different experimental conditions were adopted. The listed adsorbents without

576 doubt showed high adsorption capacities, under optimized condition of work, however they required
577 pre-treatment (increasing the associated costs) if compared with our work (in same case hard acid
578 conditions of work far from cleaner and sustainable production technologies are reported).
579 Conversely, a greener approach is presented in this paper avoiding the use of particular treatments of
580 the adsorbent and hard condition of work.

581

ADSORBENT	**Q_{MAX} (mg×g^{-1})**	**REFERENCES**
$MnFe_2O_4$/activated carbon	283[a]	Shao et al., 2012
Graphene Oxide	313,5	Gao et al., 2012
Rice husk ash	4	Liu et al., 2012
magnetic, macro-reticulated cross-linked chitosan	21	Oladoja et al., 2014
Amino-Fe(III) functionalizated SBA15	46[a]	Zhang et al., 2015
Graphene oxide/Calcium alginate composite fibers	312,5	Fan et al., 2016
KOH-activated graphene	532,6	Ma et al., 2017
magnetic chitosan nanoparticles	78,11	Raeiatbin et al., 2017
Composite cryogel	2042	Yeşilova et al., 2018
Oxidized activate carbon	634	Qin et al., 2018
Spent coffee ground	64,89 123,46	Dai et al., 2019
Zeolitic imidazolated framework	446,9	Dehgan et al.,2019

mAL/CH/TiO_2	0,96 (× cycle)	This study

a: these values have been adopted by literature and transformed in mg/g

Table 2: *Comparison of Q_{max} values obtained in literature for removal of TC from water by using different adsorbent materials.*

Further, the works listed in **Table 2** did not investigate the possibility to recover the pollutant or perform consecutive cycles of adsorption and/or desorption by using mild conditions of work, *i.e.* in presence of salts to desorb TC. So, the reported adsorbents could be considered secondary pollutants and should be removed from the environment. On the other hand, with the present work, the TC is recovered proposing a safer and recyclable ecofriendly adsorbent. As alternative, the TC can be photodegraded when blocked inside the adsorbent proposing the reuse of mAL/CH/TiO_2. Although, during this study the obtained Q_{max}, from the Langmuir isotherm, was lower than values reported for other materials, the possibility to reuse the adsorbent for several consecutive cycles of adsorption can be considered advantageous beside the TC recover. Indeed, the economic impact of the proposed technology, if compared with the previous literature, can be beneficial for real applications. The associated costs are very low: 1€ per gram of chitosan and 0.11€ per gram of alginate. Further, the use of salts for the TC recovery can be a positive aspect, considering that the associated cost of $MgCl_2 \cdot 6H_2O$ is approximately 35 € per 100 g. It should be considered that the price reported by Sigma Aldrich for the pollutant is about 200 €/100g, so a net gain in the recovery of the TC should be obtained. In conclusion, hard conditions of work are avoided by adopting green and safer technologies according to Green Chemistry and Green Economy.

4. CONCLUSIONS

In this work, a photoactive composite adsorbent is proposed as material for the removal of EPs from wastewater, using tetracycline as model molecules. The proposed bioadsorbent was composed by alginate microbeads wrapped with chitosan and enriched with TiO_2 commercial nanoparticles (mAL/CH/TiO_2). Similar materials were already used for textile dyes and heavy metal removal, but in this case, it was applied as adsorbent for removing/degrading a different class of pollutants. The synergic use of natural biopolymers and commercially available TiO_2 made this material interesting in terms of low costs and eco-sustainability. To induce the TC photodegradation, AOPs were used; on the other hand, to recover the pollutant, $MgCl_2$ was suggested. Unfortunately, the presence of Mg^{2+} induced the material destruction due to the polymeric network breaking. For this reason, besides the investigated adsorption capacities, the adsorbent was also subjected to AOPs, enabling the possibility to recover the adsorbent material for recycling it, photo-removing the pollutant. It is aimed that the reuse of the recovered pollutant and/or adsorbent increases the social awareness about the benefits that could be obtained protecting the environment through the reuse of products. The recover in an environmental-friendly way could be a safer approach to protect the environment. Indeed, the emerging of prevention-based approaches as Cleaner Production and Pollution Prevention do not only offer environmental advantages, but also include cost benefits.

5. REFERENCES

Abdel-Ghani, N.T., Rawash, E.S.A., El-Chaghaby, G.A., 2016. Equilibrium and kinetic study for the adsorption of p-nitrophenol from wastewater using olive cake based activated carbon. Global J. Environ. Sci. Manage. 2(1), 11-18. DOI: 10.7508/gjesm.2016.01.002

Abdolmaleki, A.Y., Zilouei, H., Khorasani, S.N., Zargoosh, K., 2018. Adsorption of tetracycline from water using glutaraldehyde-crosslinked electrospun nanofibers of chitosan/poly(vinyl alcohol). Water Sci. Technol. 77(5), 1324-1335. DOI: 10.2166/wst.2018.010.

Abdulghani, A.J., Jasim, H.H., Hassan, A.S., 2013. Determination of Tetracycline in Pharmaceutical Preparation by Molecular and Atomic Absorption Spectrophotometry and High Performance Liquid Chromatography via Complex Formation with Au(III) and Hg(II) Ions in Solutions. Int. J. Anal. Chem. Article ID 305124. http://dx.doi.org/10.1155/(2013)/305124.

Belayutham, S., Gonzalez, V.A., Yiu, T.W., 2016. A cleaner production-pollution prevention based framework for construction site induced water pollution, J. Clean. Prod. 135, 1363-1378. DOI: 10.1016/j.jclepro.2016.07.003.

Berhane, T.M., Levy, J., Krekeler, M.P.S., Danielson, N.D., 2017. Kinetic sorption of contaminants of emerging concern by a palygorskite-montmorillonite filter medium, Chemosphere 176, 231-242. DOI: 10.1016/j.chemosphere.2017.02.068.

Caroni, A.L.P.F., de Lima, C.R.M., Pereira, M.R., Fonseca, J.L.C., 2009. The kinetics of adsorption of tetracycline on chitosan particles. J. Colloid Interf. Sci. 340, 182–191. DOI: 10.1016/j.jcis.2009.08.016

Chen, Y.J., Wang, F.H., Duan, L.C., Yang, H. Gao, J., 2016. Tetracycline adsorption onto rice husk ash, an agricultural waste: Its kinetic and thermodynamic studies. J. Mol. Liq. 222, 487–494. DOI: 10.1016/j.molliq.2016.07.090.

Dai, Y.J., Zhang, K.X., Meng, X.B., Li, J.J., Guan, X.T., Sun, Q.Y., Sun, Y., Wang, W.S., Lin, M., Liu, M., Yang, S.S., Chen, Y.J., Gao, F., Zhang, X., Liu, Z.H., 2019. New use for spent coffee ground

as an adsorbent for tetracycline removal in water. Chemosphere 215, 163-172. DOI: 10.1016/j.chemosphere.2018.09.150.

Dehghan, A., Zarei, A., Jaafari, J., Shams, M., Khaneghah, A.M., 2019. Tetracycline removal from aqueous solutions using zeolitic imidazolate frameworks with different morphologies: A mathematical modelling. Chemosphere 217, 250-260. DOI: 10.1016/j.chemosphere.2018.10.166.

Dong, H.R., Jiang, Z., Zhang, C., Deng, J.M., Hou, K.J., Cheng, Y.J., Zhang, L.H., Zeng, G.M., 2018. Removal of tetracycline by Fe/Ni bimetallic nanoparticles in aqueous solution. J. Colloid Interf. Sci. 513, 117–125. DOI: 10.1016/j.jcis.2017.11.021.

El Haddad, M., Slimani, R., Mamouni, R., ElAntri, S., Lazar, S., 2013. Removal of two textile dyes from aqueous solutions onto calcined bones. J. Assoc. Arab Univ. Basic Appl. Sci. 14, 51–59. https://doi.org/10.1016/j.jaubas.2013.03.002.

Fan, H.T., Shi, L.Q., Shen, H., Chen, X., Xie, K.P., 2016. Equilibrium, isotherm, kinetic and thermodynamic studies for removal of tetracycline antibiotics by adsorption onto hazelnut shell derived activated carbons from aqueous media. RSC Adv. 6(111), 109983-109991. DOI: 10.1039/c6ra23346e.

Gao, Y., Li, Y., Zhang, L., Huang, H., Hu, J., Shah, S.M., Su, X., 2012. Adsorption and removal of tetracycline antibiotics from aqueous solution by graphene oxide. J. Colloid Int. Sci. 368(1), 540–546. https://doi.org/10.1016/j.jcis.2011.11.015.

Guler, U.A., Sarioglu, M., Removal of tetracycline from wastewater using pumice stone: equilibrium, kinetic and thermodynamic studies. J. Environ. Health Sci. Eng. 12(1), 79. DOI: 10.1186/2052-336X-12-79.

Günay, A., Arslankaya, E., Tosun, İ., 2007. Lead removal from aqueous solution by natural and pretreated clinoptilolite: Adsorption equilibrium and kinetics. J. Hazard. Mater. 146, 362–371. DOI: 10.1016/j.jhazmat.2006.12.034.

Hens, L., Block, C., Cabello-Eras, J. J., Sagastume-Gutierez, A., Garcia-Lorenzo, D., Chamorro, C., Herrera Mendoza, K., Haeseldonckx, D., Vandecasteele, C., 2018. On the evolution of “Cleaner

Production" as a concept and a practice. J. Clean. Prod. 172, 3323-3333. DOI: 10.1016/j.jclepro.2017.11.082.

Jiang, X., Guo, Y.H., Zhang, L.B., Jiang, W.J., Xie, R.Z., 2018. Catalytic degradation of tetracycline hydrochloride by persulfate activated with nano Fe0 immobilized mesoporous carbon. Chem. Eng. J. 341, 392-401. DOI: 10.1016/j.cej.2018.02.034.

Kurk, F., Eagan, P., 2008. The value of adding design-for-the-environment to pollution prevention assistance options. J. Clean. Prod. 16, 722-726. DOI: 10.1016/j.jclepro.2007.02.022.

Lam, W-H., Chong, M.N., Horri, B.A., Tey, B-T., Chan, E-S., 2017. Physicochemical stability of calcium alginate beads immobilizing TiO_2 nanoparticles for removal of cationic dye under UV irradiation. J. Appl. Polym. Sci. 45002. DOI: 10.1002/APP.45002;

Lee, D.W., Lim, C., Israelachvili, J.N., Hwang, D.S., 2013. Strong Adhesion and Cohesion of Chitosan in Aqueous Solutions. Langmuir 29(46), 14222–14229. DOI: 10.1021/la403124u.

Liu, J., Pu, H.M., Zhang, X., Xiao, L.X., Kan, J., Jin, C.H., 2018. Effects of ascorbate and hydroxyl radical degradations on the structural, physicochemical, antioxidant and film forming properties of chitosan. Int. J. Biol. Macromol. 114, 1086–1093. DOI: 10.1016/j.ijbiomac.2018.04.021

Liu, P., Liu, W.J., Jiang, H., Chen, J.J., Li, W.W., Yu, H.Q., 2012. Modification of bio-char derived from fast pyrolysis of biomass and its application in removal of tetracycline from aqueous solution. Bioresour. Technol. 12, 235–240. DOI: 10.1016/j.biortech.2012.06.085.

Lopez-Penalver, J.J., Sanchez-Polo, M., Gomez-Pacheco, C.V., Rivera-Utrilla, J., 2010. Photodegradation of tetracyclines in aqueous solution by using UV and UV/H2O2 oxidation processes. J. Chem. Technol. Biotechnol. 85, 1325–1333. DOI: 10.1002/jctb.2435.

Lu, T.T., Zhu, Y.F., Qi, Y.X., Wang, W.B., Wang, A.Q., 2018. Magnetic chitosan–based adsorbent prepared via Pickering high internal phase emulsion for high-efficient removal of antibiotics. Int. J. Biol. Macromol. 106, 870-877. DOI: 10.1016/j.ijbiomac.2017.08.092.

Ma, J., Sun, Y., Yu, F., 2017. Efficient removal of tetracycline with KOH-activated graphene from aqueous solution. Roy Soc Open Sci. 4, 170731. http://dx.doi.org/10.1098/rsos.170731.

Martins, A.C., Pezoti, O., Cazetta, A.L., Bedin, K.C., Yamazaki, D.A.S., Bandoch, G.F.G., Asefa, T., Visentainer, J.V., Almeida, V.C., 2015. Removal of tetracycline by NaOH-activated carbon produced from macadamia nut shells: Kinetic and equilibrium studies. Chem. Eng. J. 260, 291–299. DOI: 10.1016/j.cej.2014.09.017.

Moussavi, G., Khosravi, R., 2011. The removal of cationic dyes from aqueous solutions by adsorption onto pistachio hull waste. Chem. Eng. Res. Des. 89(10), 2182–2189. DOI: 10.1016/j.cherd.2010.11.024.

Nawi, M.A., Jawad, A.H., Sabar, S., Ngah, W.S.W., 2011. Photocatalytic-oxidation of solid state chitosan by immobilized bilayer assembly of TiO_2–chitosan under a compact household fluorescent lamp irradiation. Carbohyd. Polym. 83, 1146–1152. DOI: 10.1016/j.carbpol.2010.09.044.

Oladoja, N.A., Adelagun, R.O.A., Ahmad, A.L., Unuabonah, E.I., Bello, H.A., 2014. Preparation of magnetic, macro-reticulated cross-linked chitosan fortetracycline removal from aquatic systems. Colloids Surf. B 117, 51–59. DOI: 10.1016/j.colsurfb.2014.02.006.

Pakdel, P.M., Peighambardoust, S.J., 2018. A review on acrylic based hydrogels and their applications in wastewater treatment. J. Environ. Manag. 217, 123-143. DOI: 10.1016/j.jenvman.2018.03.076.

Qin, Q.D., Wu, X., Chen, L.W., Jiang, Z.S., Xu, Y., 2018. Simultaneous removal of tetracycline and Cu(II) by adsorption and coadsorption using oxidized activated carbon. RSC Adv. 8, 1744. DOI: 10.1039/c7ra12402c.

Raeiatbin, P., Açıkel, Y. S., 2017. Removal of tetracycline by magnetic chitosan nanoparticles from medical wastewaters. Desalin. Water Treat. 73, 380–388. DOI: 10.5004/dwt.2017.20421.

Ragazzoni, A.E., 2020. Adsorption kinetics at solid/aqueous solution interfaces: On the boundaries of the pseudo-second order rate equation. Colloids Surf A 585, 124093. DOI: 10.1016/j.colsurfa.2019.124093

Rizzi, V., Lacalamita, D., Gubitosa, J., Fini, P., Petrella, A., Romita, R., Agostiano, A., Gabaldón, J. A., Fortea Gorbe, M. I., Gómez-Morte, T., Cosma, P., 2019a. Removal of tetracycline from polluted water by chitosan-olive pomace adsorbing films. Sci. Total Env. 693, 133620. DOI: 10.1016/j.scitotenv.2019.133620.

Rizzi, V., Romanazzi, F., Gubitosa, J., Fini, P., Romita, R., Agostiano, A., Petrella, A., Cosma, P., 2019b. Chitosan Film as Eco-Friendly and Recyclable Bio-Adsorbent to Remove/Recover Diclofenac, Ketoprofen, and their Mixture from Wastewater. Biomolecules 9(10), 571. DOI: 10.3390/biom9100571.

Safari, G.H., Hoseini, M., Seyedsalehi, M., Kamani, H., Jaafari, J., Mahvi, A.H., 2015. Photocatalytic degradation of tetracycline using nanosized titanium dioxide in aqueous solution. Int. J. Environ. Sci. Technol. 12, 603–616. DOI: 10.1007/s13762-014-0706-9.

Semeraro, P., Fini, P., D'Addabbo, M., Rizzi, V., Cosma, P., 2017. Removal from wastewater and recycling of azo textile dyes by alginate-chitosan beads. International Journal of Environment, Agriculture and Biotechnology (IJEAB) 2(4), 1835-1850. http://dx.doi.org/10.22161/ijeab/2.4.48.

Shahmohammadi-Kalalagh, S., Babazadeh, H., Nazemi, A.H., Manshouri, M., 2011. Isotherm and Kinetic Studies on Adsorption of Pb, Zn and Cu by Kaolinite. Caspian J. Environ. Sci. 9, 243–255. http://research.guilan.ac.ir/cjes.

Shao, L.N., Ren, Z.M., Zhang, G.S., Chen, L.L., 2012. Facile synthesis, characterization of a MnFe2O4/activated carbon magnetic composite and its effectiveness in tetracycline removal, Mater. Chem. Phys. 135, 16-24. DOI: 10.1016/j.matchemphys.2012.03.035.

Tan, P.Y., Tan, T.B., Chang, H.W., Tey, B.T., Chan, E.S., Lai, O.M., Baharin, B.S., Nehdi, I.A., Tan, C.P., 2018. Effects of storage and yogurt matrix on the stability of tocotrienols encapsulated in chitosan-alginate microcapsules. Food Chem 241, 79–85. DOI: 10.1016/j.foodchem.2017.08.075.

Thakur, S., Sharma, B., Verma, A., Chaudhary, J., Tamulevicius, S., Thakur, V.K., 2018. Recent progress in sodium alginate based sustainable hydrogels for environmental applications. J. Clean. Prod. 198, 143-159. DOI: 10.1016/j.jclepro.2018.06.259

Tien, S., Ramarao, B.V., 2014. Further examination of the relationship between the Langmuir kinetics and the Lagergren and the second-order rate models of batch adsorption, Sep. Purif. Technol 136, 303–308. DOI: 10.1016/j.seppur.2014.08.013

Vega, E., Valdes, H., 2018. New evidence of the effect of the chemical structure of activated carbon on the activity to promote radical generation in an advanced oxidation process using hydrogen peroxide, Microporous Mesoporous Mater. 259, 1-8. DOI: 10.1016/j.micromeso.2017.09.018.

Yesilova, E., Osman, B., Kara, A., Ozer, E.T., 2018. Molecularly imprinted particle embedded composite cryogel for selective tetracycline adsorption. Sep. Purif. Technol. 200, 155–163. 10.1016/j.seppur.2018.02.002.

Zhang, Z., Lan, H., Liu, H., Qu, J., 2015. Removal of tetracycline antibiotics from aqueous solution by amino-Fe (III) functionalized SBA15. Colloid Surf. A 471, 133–138. DOI: 10.1016/j.colsurfa.2015.02.018.

Zhou, Y., Yang, Q., Zhang, D.N., Gan, N., Li, Q.P., Cuan, J., 2018. Detection and removal of antibiotic tetracycline in water with a highly stable luminescent MOF. Sens. Actuators B 262, 137–143. DOI: 10.1016/j.snb.2018.01.218.

Zhu, H.T., Chen, T., Liu, J.Q., Li, D., 2018. Adsorption of tetracycline antibiotics from an aqueous solution onto graphene oxide/calcium alginate composite fibers. RSC Adv. 8, 2616-2621. DOI: 10.1039/c7ra11964j.

Zhu, X.D., Liu, Y.C., Qian, F., Zhou, C., Zhang, S.C., Chen, J.M., 2014. Preparation of magnetic porous carbon from waste hydrochar by simultaneous activation and magnetization for tetracycline removal. Bioresour. Technol. 154, 209–214. DOI: 10.1016/j.biortech.2013.12.019.